A Class of Multivariate Denoising Algorithms Based on Synchrosqueezing

Alireza Ahrabian and Danilo P. Mandic, *Fellow, IEEE*

***Abstract*—Univariate thresholding techniques based on high resolution time-frequency algorithms, such as the synchrosqueezing transform, have emerged as important tools in removing noise from real world data. Low cost multichannel sensor technology has highlighted the need for direct multivariate denoising, and to this end, we introduce a class of multivariate denoising techniques based on the synchrosqueezing transform. This is achieved by partitioning the time-frequency domain so as to identify a set of modulated oscillations common to the constituent data channels within multivariate data, and by employing a modified universal threshold in order to remove noise components, while retaining signal components of interest. This principle is used to introduce both the wavelet and Fourier based multivariate synchrosqueezing denoising algorithms. The performance of the proposed multivariate denoising algorithm is illustrated on both synthetic and real world data.**

***Index Terms*—Multivariate signal analysis, multivariate signal denoising, short-time Fourier transform, synchrosqueezing transform, wavelet denoising.**

I. Introduction

REAL-WORLD data is often contaminated with noise and it is widely accepted that noise characterization is best performed at the level of the instantaneous frequency. Existing denoising algorithms range from adaptive filtering based methods, such as the least mean square (LMS) algorithm [1], to more sophisticated multiscale methods based on the discrete wavelet transform (DWT) [2] and empirical mode decomposition (EMD) [3]. In particular, multiscale denoising algorithms have found numerous applications ranging from geophysical engineering [4] to location estimation in communications systems [5].

Due to their low resolution at high frequency, wavelet based denoising algorithms [2] are best suited for the separation of additive noise from a signal of interest that occupies lower frequency bands. This is achieved by a decomposition into a set of scales separated in frequency, whereby the noise component is typically present across scales and the signal of interest occupies a low frequency subset of the wavelet scales. Then, denoising is carried out by rejecting the frequency bands corresponding to noise (typically performed by thresholding), while preserving the frequency bands that contain the signal of interest. A popular threshold is the universal thresholding technique proposed in [2], [6], while a multivariate extension of the univariate wavelet denoising technique has been proposed in [7]. This was achieved by using principal component analysis (PCA) in combination with conventional univariate wavelet denoising, aiming to exploit the inter-channel dependencies in multivariate data.

The wavelet transform is a projection based decomposition algorithm that is fundamentally limited in resolving oscillatory features that occur simultaneously both in time and frequency. An alternative data driven approach to time-frequency analysis was recently introduced in [8], termed the empirical mode decomposition (EMD), that adaptively decomposes a signal into a set of localized amplitude/frequency modulated (AM/FM) oscillations termed intrinsic mode functions (IMFs). Recently, EMD-based denoising algorithms have emerged [3], these modify the universal thresholding criterion, as well as the thresholding characteristics, to adapt the denoising techniques in [2], [9] for EMD. Denoising methods based on EMD have been shown to outperform the wavelet transform [3], [10], while a recent multivariate extension of EMD (MEMD) [11] has been successfully applied to artifact removal in electroencephalography (EEG) [12].

Recently, a reassignment technique termed the synchrosqueezing transform (SST) [13]–[16], was introduced to produce highly localized time-frequency representations of modulated oscillations [17]–[20]. The SST is a post-processing technique that enhances the localization properties of conventional linear projection based methods such as the continuous wavelet transform (CWT) and short-time Fourier transform (STFT) [21] by reassigning the energies of time-frequency coefficients around the frequency of oscillations present in the signal at hand. Inspired by the synchrosqueezing transform, the work in [22] introduced a denoising technique that outperformed both the empirical mode decomposition and wavelet transform in recovering modulated oscillations in noise, however, the method was defined for univariate signals.

To this end, we here propose a multivariate denoising algorithm that employs synchrosqueezing for both the CWT and STFT in order to identify a set of modulated oscillations common to all data channels within a multivariate signal. Upon partitioning the time-frequency domain, a thresholding technique suited for the multivariate oscillatory framework is introduced and is applied to the modulated oscillations for each data channel, enabling the removal of noise from multichannel data. Illustrative simulations verify the performance of the proposed method on both synthetic and real world data.

Manuscript received August 07, 2014; revised November 18, 2014 and January 19, 2015; accepted January 23, 2015. Date of publication February 16, 2015; date of current version March 25, 2015. The associate editor coordinating the review of this manuscript and approving it for publication was Prof. Antonio Napolitano.

The authors are with the Department of Electrical and Electronic Engineering, Imperial College London, SW7 2AZ, U.K. (e-mail: alireza.ahrabian06@imperial.ac.uk; d.mandic@imperial.ac.uk).

Color versions of one or more of the figures in this paper are available online at http://ieeexplore.ieee.org.

Digital Object Identifier 10.1109/TSP.2015.2404307

The organization of this paper is as follows. Section II introduces the univariate and multivariate wavelet denoising algorithm. Section III addresses the modulated multivariate oscillation model, Section IV describes synchrosqueezing based time-frequency techniques, while Section V presents the proposed multivariate extension of the synchrosqueezing algorithm and the corresponding denoising algorithms. Section VI assesses the performance of the algorithm through simulations.

II. Wavelet Denoising Techniques

A. Univariate Wavelet Denoising

The signal denoising problem. Consider an observation, $s(t)$, of a signal of interest, $x(t)$, which is contaminated with noise $n(t)$, that is

$$s(t) = x(t) + n(t), \tag{1}$$

The objective is to remove as much as possible the effects of the additive noise component, while preserving the signal of interest. Multiscale techniques, such as the discrete wavelet transform, decompose a signal into multiple frequency bands (scales) [9], by projecting the signal across a set of orthogonal basis functions. It is usually assumed that the signal of interest is localized across a small set of frequency scales, while the noise signal is present across all scales (assuming that the noise process is broadband). By employing a threshold, scales corresponding to noise are removed and the scales containing the signal are preserved. The two popular methods used for thresholding are the hard and soft thresholding, and are given respectively by

$$F_H(x) = \begin{cases} x, & |x| > T \\ 0, & |x| \leq T \end{cases} \tag{2}$$

and

$$F_X(x) = \begin{cases} \operatorname{sgn}(x)\left(|x| - T\right), & |x| > T \\ 0, & |x| \leq T \end{cases} \tag{3}$$

where the symbol $\operatorname{sgn}(\cdot)$ refers to the sign function. An optimal threshold T that removes noise components with a high probability is known as the universal threshold [2], [6], given by

$$T = \sigma\sqrt{2\ln L}, \tag{4}$$

where σ is the standard deviation of noise and L is the length of the signal. A modified universal threshold has been proposed in [3], as a multiple of the original universal threshold, that is

$$T_{mod} = C\sigma\sqrt{2\ln L}, \tag{5}$$

where C is a positive constant. It has the advantage of being able to fine-tune the original universal threshold for signal decomposition algorithms other than the DWT [3].

B. Multivariate Wavelet Denoising

Consider the multivariate extension of the signal denoising problem in (6), given by

$$\mathbf{x}(t) = \mathbf{s}(t) + \mathbf{n}(t) \tag{6}$$

where $\mathbf{x}(t), \mathbf{s}(t), \mathbf{n}(t) \in \mathbb{R}^N$, and N is the number of data channels. As in the univariate case, the objective is to recover the multivariate desired signal, $\mathbf{s}(t)$, by exploiting the inter-channel dependencies that may exist (either between the noise or desired signals). In order to improve denoising over the conventional application of univariate wavelet denoising applied directly to each data channel independently, the multivariate wavelet denoising (MWD) algorithm employs principal component analysis in conjunction with univariate wavelet thresholding [7], and is outlined in Algorithm 1.

Algorithm 1: Multivariate Wavelet Denoising (MWD)

1) Given an N-channel multivariate signal $\mathbf{x}(t)$, apply the DWT channel-wise at a level J, to obtain a set of discrete wavelet coefficients $\mathbf{D}_J \in \mathbb{R}^{L2^{-J}\times N}$.
2) Using the detail coefficient $\mathbf{D}_1$ obtain a covariance estimate of the noise $\mathbf{\Sigma}_c$. Carry out the eigendecomposition of the covariance, $\mathbf{\Sigma}_c = \mathbf{V}\mathbf{\Lambda}\mathbf{V}^T$. Next, carry out the following matrix multiplication, $\mathbf{D}_J\mathbf{V}$, and apply the universal threshold $T_n = \sqrt{2\lambda_n \log(L2^{-J})}$, where λ_n are the eigenvalues for each channel index n.
3) Apply the inverse of the projection, $\mathbf{V}^T$, to the coefficients where the universal threshold was applied, and then make an inverse of the wavelet transform in order to obtain the denoised signal $\hat{\boldsymbol{x}}(t)$.
4) Carry out PCA on the reconstructed signal, $\hat{\boldsymbol{x}}(t)$, and by using an appropriate rule, retain the most significant principal components.

III. Modulated Multivariate Oscillations

Many real world univariate signals can be modeled by the modulated oscillation model

$$x(t) = a(t)\cos\phi(t) \tag{7}$$

where $a(t)$ and $\phi(t)$ are respectively the instantaneous amplitude and phase; the derivative of the instantaneous phase is referred to as the instantaneous frequency $\phi'(t)$. In order to identify a unique pair for $a(t)$ and $\phi(t)$, the work in [23] employed the Hilbert transform, to generate a complex analytic signal

$$x_+(t) = a(t)e^{i\phi(t)} \tag{8}$$

where $a(t)$ and $\phi(t)$ can be identified using complex algebra. For signals with slowly varying instantaneous amplitudes and frequencies, time-frequency algorithms aim to localize oscillatory components of the form (7), while spreading out the energy of the noise components in the time-frequency plane; this is the basis of univariate signal denoising algorithms [22]. In order to extend this concept for the analysis of multichannel signals, a multivariate extension of the univariate modulated oscillation model has been introduced whereby, the notion of the instantaneous frequency and amplitude were extended to model multivariate signals. Based on a multivariate analytic signal, $\mathbf{x}_+(t)$, of the following form

$$\mathbf{x}_+(t) = \begin{bmatrix} a_1(t)e^{i\phi_1(t)} \\ a_2(t)e^{i\phi_2(t)} \\ \vdots \\ a_N(t)e^{i\phi_N(t)} \end{bmatrix} \tag{9}$$

where $a_n(t)$ and $\phi_n(t)$ represent the instantaneous amplitude and phase for each channel index n, the work in [24] introduces the concept of modulated multivariate oscillation, whereby the joint oscillatory structure of the multivariate analytic signal, $\mathbf{x}_+(t)$, is modeled by the joint instantaneous frequency

$$\omega_x(t) = \frac{\Im\left\{\mathbf{x}_+^H(t)\frac{d}{dt}\mathbf{x}_+(t)\right\}}{\|\mathbf{x}_+(t)\|^2}, \tag{10}$$

where $(\cdot)^H$ is the conjugate transpose operator.

Furthermore, the joint global moments of a multivariate signal can be related to both the joint analytic spectrum and joint instantaneous frequency and bandwidth [24]. The joint analytic spectrum of a multivariate signal is determined according to

$$S_{\mathbf{x}}(\omega) = \frac{1}{E}\|\mathbf{F}_{\mathbf{x}}(\omega)\|^2 \tag{11}$$

where $\mathbf{F}_{\mathbf{x}}(\omega)$ corresponds to the channel-wise application of the Fourier transform and E denotes the total energy of the joint analytic spectrum

$$E = \frac{1}{2\pi}\int_0^\infty \|\mathbf{F}_{\mathbf{x}}(\omega)\|^2 \, \mathrm{d}\omega. \tag{12}$$

The joint analytic spectrum is then the power weighted average of the channel-wise Fourier coefficients, while the joint global mean frequency is given by

$$\overline{\omega}_{\mathbf{x}} = \frac{1}{2\pi}\int_0^\infty \omega S_{\mathbf{x}}(\omega)\, \mathrm{d}\omega, \tag{13}$$

and corresponds to the average frequency of the joint analytic spectrum. The multivariate bandwidth squared[1] is given by

$$\mathbf{B}_{\mathbf{x}}^2 = \frac{1}{2\pi}\int_0^\infty (\omega - \overline{\omega}_{\mathbf{x}})^2 S_{\mathbf{x}}(\omega)\, \mathrm{d}\omega, \tag{14}$$

where the multivariate bandwidth, $\mathbf{B}_{\mathbf{x}}$, is a measure of the standard deviation of the joint analytic spectrum. It should be noted that the global moments of the analytic spectrum can be related to the moments of joint instantaneous frequency and bandwidth as

$$\overline{\omega} = \frac{1}{E}\int_{-\infty}^\infty \|\mathbf{x}_+(t)\|^2 \omega_x(t)\, \mathrm{d}t \tag{15}$$

$$\mathbf{B}_{\mathbf{x}}^2 = \frac{1}{E}\int_{-\infty}^\infty \|\mathbf{x}_+(t)\|^2 \sigma_x^2(t)\, \mathrm{d}t, \tag{16}$$

where $\sigma_x^2(t) = \upsilon_x^2(t) + (\omega_x(t) - \overline{\omega})^2$ is the joint instantaneous second central moment and the joint instantaneous bandwidth $\upsilon_x(t)$ is given as

$$\upsilon_x(t) = \frac{\left\|\frac{d}{dt}\mathbf{x}_+(t) - i\omega_x(t)\mathbf{x}_+(t)\right\|}{\|\mathbf{x}_+(t)\|}. \tag{17}$$

The joint instantaneous bandwidth, measures the normalized error of the joint instantaneous frequency from the rate of change of the multivariate signal, whereby inserting (9) into (17), the following expression is obtained

$$\upsilon_x^2(t) = \frac{\sum_{n=1}^N (a_n'(t))^2 + \sum_{n=1}^N a_n^2(t)\left(\phi_n'(t) - \omega_x(t)\right)^2}{\sum_{n=1}^N a_n^2(t)}. \tag{18}$$

Accordingly, it can be observed that the joint instantaneous bandwidth measures both the deviations of the individual channel-wise instantaneous frequencies from the joint instantaneous frequency, along with any amplitude modulation within each channel of the multivariate signal. Assuming slowly varying instantaneous amplitudes within each channel, for a given multivariate signal with large deviations of the channel-wise instantaneous frequencies from the joint instantaneous frequency, expression (18) implies that the multivariate signal would not be well modeled as a single oscillatory structure.

IV. Synchrosqueezing Transform

The synchrosqueezing transform belongs to the class of frequency based reassignment techniques and was originally developed for the continuous wavelet transform, however, more recently the principles behind the synchrosqueezing transform[2] [21] have also be been applied to the STFT.

A. Wavelet Based Synchrosqueezing

The CWT is a time-frequency algorithm that convolves a series of finite energy oscillations, termed wavelets $\psi(t)$, with the signal of interest $x(t)$, given by

$$W(a,b) = \int a^{-1/2}\psi^*\left(\frac{t-b}{a}\right)x(t)\, \mathrm{d}t, \tag{19}$$

where $W(a,b)$ are the wavelet coefficients. A wavelet is a square integrable function that satisfies the admissibility condition

$$\int_{\mathbb{R}} \frac{\left|\hat{\psi}(\xi)\right|^2}{\xi}\, \mathrm{d}\xi < \infty \tag{20}$$

where $\hat{\psi}(\xi)$ is the Fourier transform of the mother wavelet $\psi(t)$. The scale factor a (shown in (19)) shifts the wavelet $\psi(t)$, in frequency, such that oscillatory features across different frequency scales are captured. It should also be noted that, for different scale factors a there is an overlap between the wavelet filters. This can be illustrated by the following example: given a sinusoid with a frequency ω_s, the resulting CWT coefficients of the sinusoid will spread out around the vicinity of the scale factor $a_s = \frac{\omega_\psi}{\omega_s}$, where ω_ψ is the wavelet center frequency. In this way, the estimated instantaneous frequency present in the scales in the vicinity of $a_s = \frac{\omega_\psi}{\omega_s}$ is equal to the original frequency ω_s. It is now possible, given an estimate of the instantaneous frequency $\omega_x(a,b)$ for each scale-time pair (a,b),

$$\omega_x(a,b) = -iW(a,b)^{-1}\frac{\partial W(a,b)}{\partial b} \tag{21}$$

[1]The multivariate bandwidth squared in [25] is the joint global second central moment.

[2]In this work, when referring to both wavelet and Fourier based synchrosqueezing transforms, the following term, synchrosqueezing techniques (ST) is used.

to invert the wavelet coefficients containing the same instantaneous frequency estimates in a procedure known as synchrosqueezing [18]. Given the wavelet coefficients $W(a,b)$, the synchrosqueezing transform[3] $T(\omega,b)$ is given by

$$T(\omega,b)=\int W(a,b)a^{-3/2}\,\delta(\omega_x(a,b)-\omega)\,\mathrm{d}a, \tag{22}$$

where $\delta(\cdot)$ is the delta function.

B. Fourier Based Synchrosqueezing

The short time Fourier transform (STFT) operates by first employing a window function $w(t)$ to localize the signal in time, then the Fourier transform is applied in order to obtain the frequency content [27]. Given a signal $x(t)$ the STFT is given by

$$S(\tau,\eta)=\int w(t-\tau)x(t)e^{-i\eta t}\,\mathrm{d}t. \tag{23}$$

The instantaneous frequency for each frequency index η is calculated as follows [21]

$$\omega_S(\tau,\eta)=-iS(\tau,\eta)^{-1}\,\frac{\partial S(\tau,\eta)}{\partial\eta}. \tag{24}$$

The wavelet based SST algorithm effectively inverts the wavelet transform and maps the resulting energy into appropriate frequency bins. Accordingly, the reassignment operation using the STFT is carried out by inverting the coefficients $S(\tau,\eta)$ along the instantaneous frequency estimates $\omega_S(\tau,\eta)$. The synchrosqueezing of the STFT [21] is given by

$$T_S(\omega,\tau)=\frac{1}{w(0)}\int S(\tau,\eta)\delta\left(\omega-\omega_S(\tau,\eta)\right)\,\mathrm{d}\eta. \tag{25}$$

V. Denoising Using Multivariate Extension of Synchrosqueezing Techniques (ST)

The work in [7] introduced a multivariate extension of the univariate wavelet denoising algorithm in a statistical framework, due the use of principal component analysis in processing the inter-channel dependencies. Recently, the notion of the modulated multivariate oscillation has been introduced in [24], such that modulated oscillations in multiple channels are modeled by a single oscillatory structure that captures the joint instantaneous amplitude and frequency of the multivariate signal. Inspired by the modulated multivariate oscillation model, a multivariate thresholding technique was also proposed [24]. We next propose a multichannel extension of the relevant algorithms, by partitioning the time-frequency domain into a set of V frequency bands $\{\omega_v\}_{v=1,\ldots,V}$, where each frequency band contains oscillatory components that are matched across multiple channels. Along with the proposed thresholding technique, a multivariate denoising algorithm is also developed.

A. Partitioning of the Time-Frequency Domain

Consider a multivariate signal $\mathbf{x}(t)$ with N data channels, where the corresponding ST coefficients for each channel are given by $T_n(\omega,b)$. The proposed technique for partitioning the ST coefficients along frequency uses a multivariate extension of a frequency tiling technique proposed in [28] based on multivariate bandwidth, so as to identify a set of modulated multivariate oscillations [29] that are well separated in frequency. We first propose to partition along frequency the time-frequency domain into 2^l equal width frequency bands, as shown in Fig. 1, where each frequency band is given by

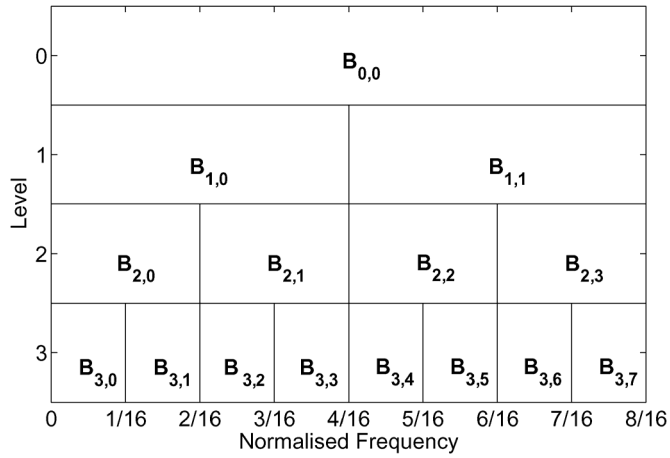

Fig. 1. The multivariate bandwidth of the partitioned frequency domain given by $\mathbf{B}_{l,m}$, where l corresponds to the level of the frequency band ($L_s=5$ typically), and m is the frequency band index.

$$\omega_{l,m}=\left[\frac{m}{2^{l+1}},\frac{m+1}{2^{l+1}}\right], \tag{26}$$

where $l=0,\ldots,L_s$, corresponds to the *level* of the frequency bands ($L_s=5$ typically) and $m=0,\ldots,2^l-1$ is the *index* of the frequency band. The multivariate bandwidth $\mathbf{B}_{l,m}$ is then calculated for a given frequency band $\omega_{l,m}$, where $\omega_{l,m}$ is split into two frequency subbands $\omega_{l+1,2m}$ and $\omega_{l+1,2m+1}$, as follows [28]:

- If the frequency band $\omega_{l,m}$ contains a multivariate monocomponent signal, then, $\mathbf{B}_{l,m}\leq\mathbf{B}_{l+1,2m}+\mathbf{B}_{l+1,2m+1}$, that is, $\omega_{l,m}$, is not split into the frequency subbands.
- If each frequency subband contains separate multivariate monocomponent signals that are well separated along frequency, then $\mathbf{B}_{l,m}>\mathbf{B}_{l+1,2m}+\mathbf{B}_{l+1,2m+1}$, accordingly $\omega_{l,m}$ is split into the frequency subbands $\omega_{l+1,2m}$ and $\omega_{l+1,2m+1}$.

The first condition can be illustrated by the following example: consider a bivariate monocomponent FM signal, where the instantaneous frequency paths for each channel of the bivariate signal are shown in Fig. 2. From Fig. 2 the multivariate bandwidth $\mathbf{B}_c$ within the frequency band $0\leq f\leq 0.25$ is equal to $\mathbf{B}_c=0.3921$. Accordingly, if the frequency band is then split into two equal frequency subbands, with frequency ranges given by $0\leq f\leq 0.125$ and $0.125<f\leq 0.25$, the corresponding sum of the multivariate bandwidths within each frequency subband is equal to 0.398, where it can be observed that the sum of the multivariate bandwidths within each frequency subband is approximately equal to the multivariate bandwidth within the frequency band. This example implies that for a given multivariate modulated oscillation, the frequency variation within each partition must be less than or equal to the frequency variation without partitioning. We next demonstrate that provided sufficient frequency separation between multivariate monocomponent oscillations, the multivariate bandwidth can be used to identify such oscillations.

[3]See [26] for details on the implementation of the SST.

For example, consider a bivariate linear frequency modulated oscillation[4]

$$\mathbf{x}_+(t) = \begin{bmatrix} e^{i\phi(t)} \\ e^{i(\phi(t)+t\Delta)} \end{bmatrix}, \quad 0 \leq t \leq T, \tag{27}$$

where $\phi(t) = \omega_0 t + \frac{k}{2}t^2$, corresponds to the instantaneous phase of the linear frequency modulated signal with chirp rate k. In order to illustrate how the multivariate bandwidth is affected by the frequency separation between two separate monocomponent signals, we have included a constant frequency deviation Δ between the channels. The multivariate bandwidth of $\mathbf{x}_+(t)$ (using (15)–(17)) is given by $\mathbf{B}_{\mathbf{x}} = \sqrt{\frac{\Delta^2}{4} + \frac{k^2}{12}T^2}$, while the bandwidth in each channel is given by, $B_1 = B_2 = \frac{k}{2\sqrt{3}}T$. The resulting summation of the individual channel bandwidths is given by $B_s = B_1 + B_2 = \frac{k}{\sqrt{3}}T$, where it should be observed that for the multivariate bandwidth, $\mathbf{B}_{\mathbf{x}}$, to be greater than the sum of the individual bandwidths for each channel, B_s, the frequency deviation needs to be greater than, $\Delta > kT$. As a result, multivariate monocomponent functions that are well separated in frequency can be identified by splitting a larger frequency band into smaller frequency subbands using the multivariate bandwidth in conjunction with frequency partitioning [28].

Algorithm 2: Multivariate Time-Frequency Partitioning

1) Partition the time-frequency plane into 2^l equal-width frequency bands $\omega_{l,m}$.
2) For a given frequency band, $\omega_{l,m}$, at level l and index m, determine the multivariate bandwidth $\mathbf{B}_{l,m}$, using (11)–(14), for the following multivariate signal,

$$\mathbf{x}_t(b) = \left[\sum_{\omega \in \omega_{l,m}} T_1(\omega, b), \ldots, \sum_{\omega \in \omega_{l,m}} T_n(\omega, b) \right]^T.$$

3) Starting from $l = 0$, a frequency split is carried out if the following condition is satisfied,

$$\mathbf{B}_{l,m} > \frac{\mathbf{B}_{l+1,2m}\Lambda_{l+1,2m} + \mathbf{B}_{l+1,2m+1}\Lambda_{l+1,2m+1}}{\Lambda_{l+1,2m} + \Lambda_{l+1,2m+1}}$$

where

$$\Lambda_{l+1,2m} = \sum_{b=1}^{T} \left(A^{multi}_{l+1,2m}(b)\right)^2$$

$$\Lambda_{l+1,2m+1} = \sum_{b=1}^{T} \left(A^{multi}_{l+1,2m+1}(b)\right)^2$$

where $A^{multi}_{l+1,2m}(b)$ and $A^{multi}_{l+1,2m+1}(b)$ correspond to the multivariate instantaneous amplitudes for the respective frequency subbands and is defined by

$$A^{multi}_{l,m}(b) = \sqrt{\sum_{n=1}^{N} \left| \sum_{\omega \in \omega_{l,m}} T_n(\omega, b) \right|^2}.$$

[4]Appendix B provides an example using bivariate oscillations with a polynomial instantaneous phase.

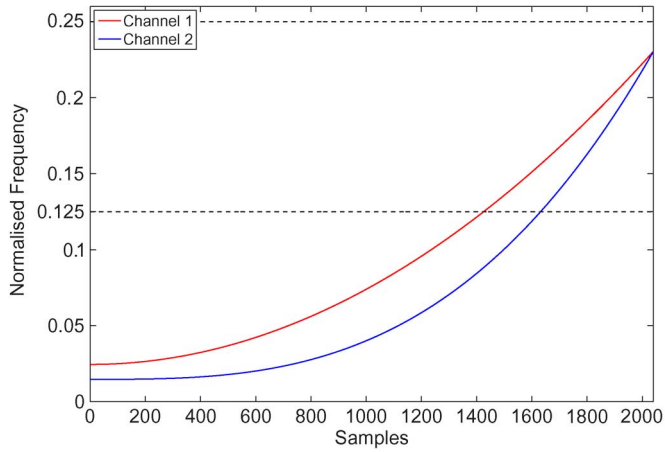

Fig. 2. The overlayed instantaneous frequency paths of a bivariate monocomponent FM signal. The instantaneous frequency of the first channel (red line) is given by, $\phi_1'(t) = 2\pi(5 + 0.42t^2)$, and the corresponding instantaneous frequency of the second channel (blue line) is given by $\phi_2'(t) = 2\pi(3 + 0.044t^3)$. The multivariate bandwidth between the frequencies $0 \leq f \leq 0.25$ is equal to 0.3921, while the sum of the individual multivariate bandwidths in the frequency partitions $0 < f \leq 0.125$ and $0.125 \leq f \leq 0.25$ is equal to 0.398.

Algorithm 2 outlines the procedure for identifying a set of adaptive frequency bands given by $\{\omega_v\}_{v=1,\ldots,V}$, where V is the number of oscillatory scales and $\omega_1 > \omega_2 > \cdots > \omega_V$. It should be noted that the condition required for splitting frequency bands, that is (3), has been modified in Algorithm 2 so as to factor the total energy of the frequency subbands, such that subbands with negligible signal content are not considered. Finally, as the partitioning algorithm requires accurate estimation of the multivariate bandwidth which in turn depends upon accurate estimation of the joint global mean frequency, for the STFT based synchrosqueezing method, the joint global mean frequency may not be accurately estimated and therefore incomplete partitioning may occur when processing multicomponent modulated multivariate oscillations.

Algorithm 3: Multivariate Denoising using ST

1) Given an N-channel multivariate signal $\mathbf{x}(t)$, apply the ST channel-wise in order to obtain the coefficients $T_n(\omega, b)$.
2) Determine a set of partitions based on the multivariate bandwidth, such that the ST coefficients $T_n(\omega, b)$ are separated into a set of oscillatory scales $F_{n,v}(b)$, for each channel index n and scale index v.
3) For a noise process, determine the variance $\sigma^2_{n,v}$ for each channel and scale, shown in Appendix C.
4) Using the multivariate instantaneous amplitude $A^{multi}_v(b)$, carry out thresholding as shown in (30).

B. Denoising Using Synchrosqueezing Techniques

Consider a multivariate signal $\mathbf{x}(t)$, with the corresponding partitioned ST coefficients, $F_{n,v}(b)$, given by

$$F_{n,v}(b) = \sum_{\omega \in \omega_v} T_n(\omega, b), \tag{28}$$

where n denotes the channel index, while v corresponds to the oscillatory scale. We first need to estimate the variance of the noise signal in each oscillatory scale. Recall that for the discrete wavelet transform, the variance of noise in each oscillatory scale remains constant, while for the partitioned ST coefficients the variance of the noise varies across scale—an expression for the power within each oscillatory scale is provided in Appendix C where only the estimate of the noise variance in the first oscillatory scale $F_{n,1}$ is required.

The conventional hard and soft thresholding applied to the ST coefficients would yield discontinuities in the recovered signal of interest even in the absence of noise, which is not desirable. To this end, to capture the inter-channel dependencies that arise between multichannel signals we propose a thresholding technique that employs the multivariate instantaneous amplitude

$$A_v^{multi}(b) = \sqrt{\sum_{n=1}^{N} |F_{n,v}(b)|^2}. \tag{29}$$

Such thresholding is then directly applied to the multivariate instantaneous amplitude, as

$$\hat{F}_{n,v}(b) = \begin{cases} F_{n,v}(b), & A_k^{multi}(b) > T_{mod} \\ 0, & A_k^{multi}(b) \leq T_{mod} \end{cases} \tag{30}$$

where T_{mod} is the modified universal threshold (typical values for C given in (5), is between[5] 0.1–0.3). The recovered signal can then be obtained by summing the coefficients, $\hat{F}_{n,v}(b)$, as follows

$$\hat{s}_n(b) = \sum_{v=1}^{V} \hat{F}_{n,v}(b) \tag{31}$$

where $\hat{s}_n(b)$ corresponds to the denoised signal for each channel. A summary of the proposed multivariate denoising algorithm is given in Algorithm 3.

VI. Simulations

The performance of the proposed multivariate wavelet synchrosqueezing denoising (MWSD) algorithm and the multivariate STFT based synchrosqueezing denoising[6] (MFSD) algorithm is next demonstrated on both synthetic and real world signals. The proposed algorithm was compared to MWD, BEMD denoising (BEMD-D) algorithm, which combines the proposed multivariate threshold within BEMD [30], and also the multivariate partitioned CWT in combination with the proposed multivariate threshold (MCWT-D). The synthetic signals consist of monocomponent sinusoids as well as a multicomponent frequency modulated oscillation, in varying levels of noise. The three real world case studies were: accelerometer data pertaining to arm swings during walk, oceanographic data collected from freely drifting floats, and motor imagery data in EEG based brain computer interface (BCI).

[5]The values were selected based on a qualitative assessment of both the reconstructed SNR and smoothness of the resulting denoised signals, where priority was given on smooth denoised signals with no spurious noise artifacts in the recovered signal.

[6]The MATLAB code for both MWSD and MFSD algorithms are available on request.

A. Denoising Monocomponent Sinusoidal Oscillations

The first set of simulations considers a bivariate sinusoidal oscillation in white Gaussian noise, given by

$$\mathbf{y}_S(t) = \begin{bmatrix} \cos(2\pi f t) \\ \cos\left(2\pi f t + \frac{\pi}{2}\right) \end{bmatrix} + \begin{bmatrix} n_1(t) \\ n_2(t) \end{bmatrix}, \tag{32}$$

where the sinusoidal oscillation was sampled at 1000 Hz, and the corresponding frequency of the sinusoids are $f = [5, 40, 100]$ Hz. Fig. 3(a) shows the reconstruction SNRs (averaged for both channels) corresponding to the sinusoids in varying levels of white Gaussian noise, with equal SNR between the two channels. It can be observed from Fig. 3(a) that the proposed MWSD method consistently outperforms the MWD and MCWT-D algorithms,[7] especially at higher frequencies; furthermore the proposed MWSD algorithm outperforms the BEMD-D algorithm for both high and low frequencies. For the bivariate sinusoidal oscillation with a frequency of 100 Hz, the reconstruction SNR for the proposed method decayed rapidly when the input SNR falls below 0 dB. This is due to the underlying behavior of SST (including CWT) at high frequencies in the presence of noise; the wavelet transform has a dyadic filter bank structure such that at higher frequencies the bandwidth of the wavelet filter is wider. As the SST requires an accurate estimate of the instantaneous frequency within each wavelet coefficient in order to accurately reassign, the accuracy in the estimation of the instantaneous frequency degrades at higher frequencies in the presence of broadband noise. From Fig. 3(a) it can be seen that the performance of the MFSD algorithm is also frequency dependent; for low frequencies the MFSD was outperformed by both the MWSD and MWD algorithms. This is due to the incomplete partitioning of the STFT based synchrosqueezing coefficients into modulated oscillations. For high frequencies, the MFSD outperformed both the MWD and MWSD, as the STFT does not have the dyadic filter bank property of the CWT, and exhibits uniform resolution dependent only on the length of the data window. Accordingly, the estimated instantaneous frequency for higher frequencies in the presence of noise did not degrade, and STFT based synchrosqueezing coefficients did not depend as much on the frequency of the sine waves. Finally, the multivariate partitions and threshold were also applied to STFT (not shown in the figures), where MFSD outperformed STFT denoising for higher frequencies, however for low frequencies, due to incomplete partitioning of MFSD, the STFT based method outperformed MFSD.

For rigor, a variation of the previous simulation for unbalanced powers in data channels was next considered. We only consider the proposed MWSD algorithm, similar results can also be obtained using the MFSD algorithm. Consider a bivariate sinusoidal oscillation (as in (32)) with frequencies $f = [40, 100, 150]$ Hz, in white Gaussian noise, where an inter-channel power imbalance was introduced both at the SNR in each channel was different. The SNR of the second channel was fixed at 20 dB, while the SNR of the first channel was varied between -10 to 20 dB. Fig. 3(b) compares the performance of proposed denoising algorithm for both the balanced inter-

[7]This is due to the energy of the oscillatory scales when partitioning CWT which may not be localized completely within the partitions due to the trade-off between the time and frequency resolution.

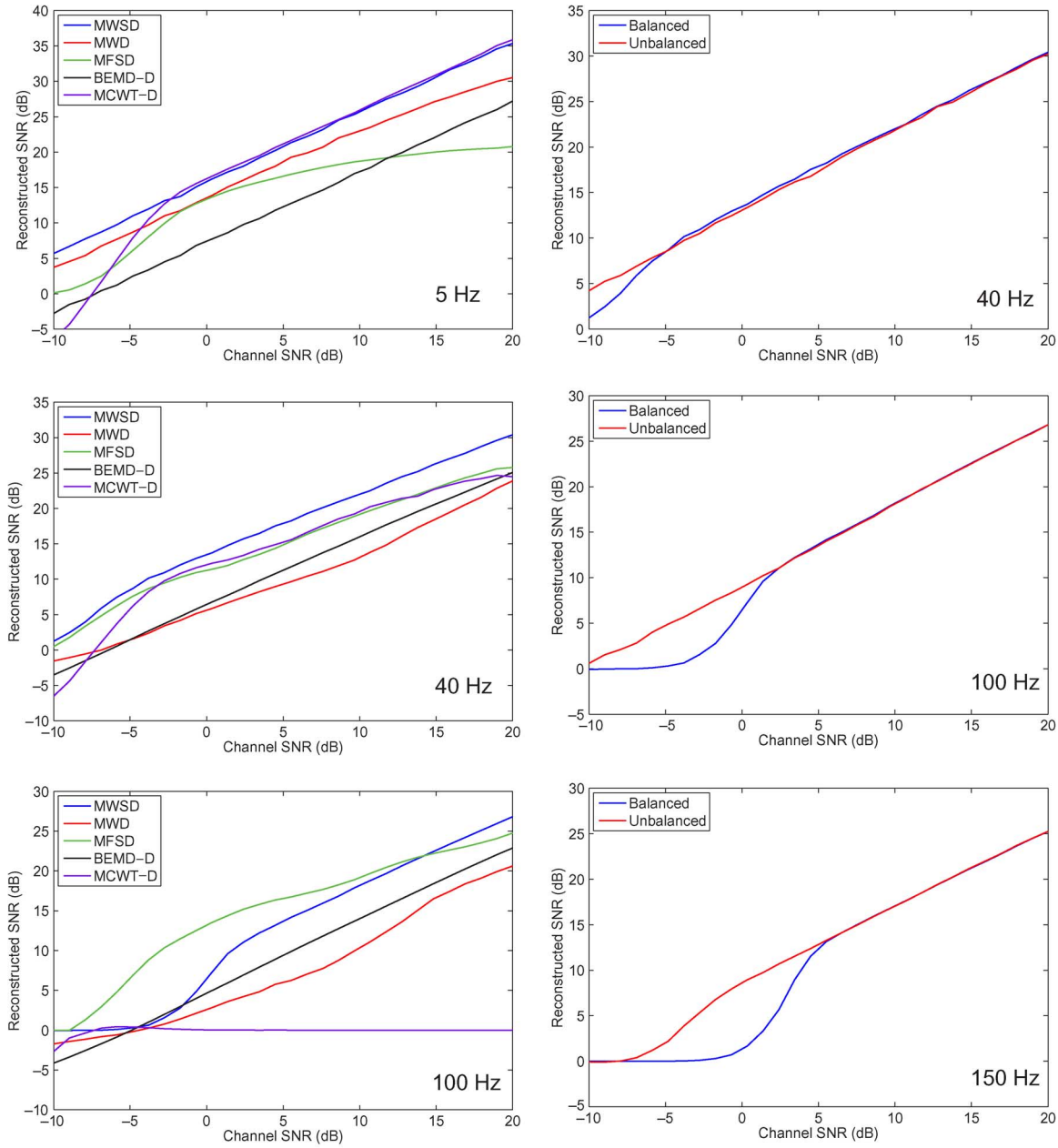

(a) Balanced channel SNR (b) Unbalanced channel SNR

Fig. 3. Denoising of bivariate sinusoids. (a) The reconstruction SNRs of the denoised signal of interest for both the proposed methods (MWSD and MFSD), MWD, MCWT-D and BEMD-D algorithms for bivariate sinusoidal oscillations in white Gaussian noise, and with equal channel SNRs. (b) The reconstruction SNR for bivariate sinusoidal oscillations in noise using the MWSD algorithm. The blue line corresponds to the reconstruction error for equal SNRs in data channels, while the red line corresponds to the reconstruction error for different SNRs in data channels. (a) Balanced channel SNR; (b) unbalanced channel SNR.

channel SNR and the unbalanced inter-channel SNR scenario (for the unbalanced bivariate signal the reconstruction error in the first channel was calculated). Observe that for the frequencies 100 Hz and 150 Hz and for high noise powers, the performance of the proposed method for the unbalanced inter-channel SNR case showed a significant improvement over the balanced inter-channel SNR scenario.

B. Denoising Multicomponent Frequency Modulated Oscillations

Consider a bivariate multicomponent frequency modulated (FM) signal $y_{FM}(t)$ in white Gaussian noise (sampled at 200 Hz), where the underlying frequency modulated signals contain both a sinusoidal instantaneous frequency combined with a linear instantaneous frequency, that is

$$\mathbf{y}_{FM}(t) = \begin{bmatrix} \cos\left(\phi_1(t)\right) + \cos\left(\phi_2(t)\right) \\ \cos\left(\phi_1(t) + \frac{\pi}{2}\right) + \cos\left(\phi_2(t) + \frac{\pi}{2}\right) \end{bmatrix} + \begin{bmatrix} n_1(t) \\ n_2(t) \end{bmatrix},$$

where

$$\phi_1(t) = 2\pi\left(10t + 3.5\cos(t)\right), \quad \phi_2(t) = 2\pi(25t + 0.8t^2)$$

and $n_1(t)$, $n_2(t)$ are independent white Gaussian noise realizations. As with the previous simulation (where a sinusoidal

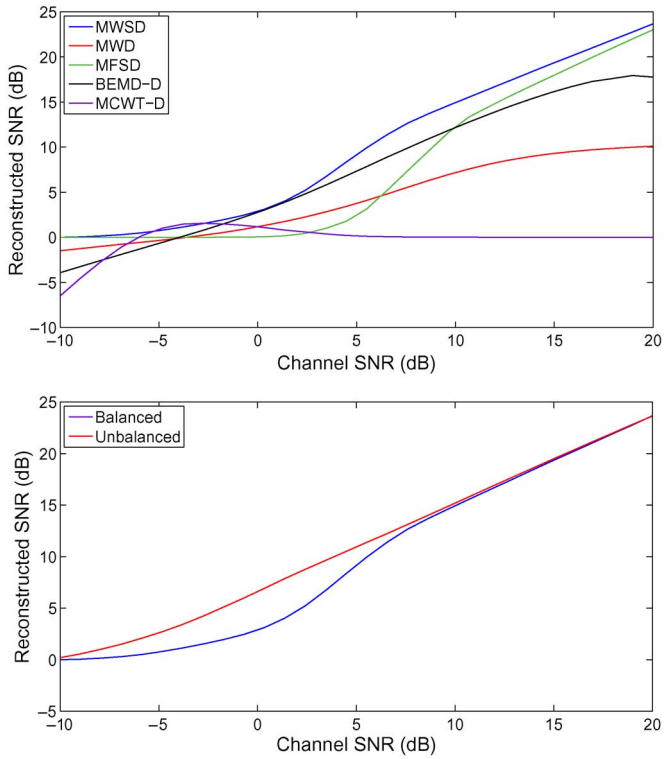

Fig. 4. The reconstruction SNRs of the bivariate multicomponent FM signal in noise for both the proposed methods (MWSD and MFSD), MPW, MCWT-D and BEMD-D algorithms (upper panel). Comparison of the proposed MWSD algorithm when processing a bivariate multicomponent FM signal with equal (balanced) and different (unbalanced) inter-channel powers (lower panel).

oscillation was considered) two cases were considered: the first case assumes that the bivariate signals have equal inter-channel SNRs, while in the second case there was an imbalance in the inter-channel SNRs. Fig. 4 (upper panel) shows that the proposed MWSD algorithm outperformed MWD, for channel SNRs greater than -5 dB, while the MWSD algorithm outperformed the BEMD denoise (BEMD-D) algorithm for input channel SNRs greater than 4 dB. Furthermore, MSWD outperformed MCWT-D algorithm for all input signal SNRs, this is due to the multicomponent signal occupying the mid- to high-frequency ranges such that the resulting CWT coefficients had lower frequency resolution. The proposed MFSD algorithm outperformed both MWD and BEMD-D algorithms for input channel SNRs of 6 dB and 10 dB respectively. For SNRs lower than -5 dB, the performance of the proposed algorithms and MWD algorithm were similar, with the BEMD-D having a lower reconstruction SNR for very low input channel SNRs. Finally, it should also be noted that MFSD outperformed multivariate STFT denoising algorithm, for very low input signal SNRs, however the performance of both methods at higher input signal SNRs were equal. Fig. 4 (lower panel) compares the performance of the proposed method (MWSD) for equal channel SNRs versus different channel SNRs in the bivariate FM signal. As the noise power increased, the reconstruction SNR for the unbalanced bivariate signal was higher than that for the balanced bivariate signal, demonstrating that the proposed algorithm is able to exploit inter-channel dependencies in order to recover the signal of interest.

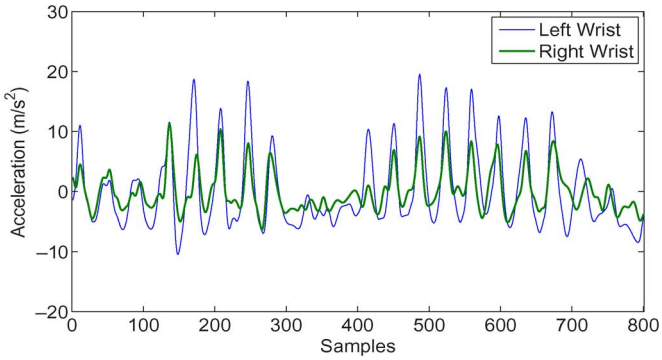

Fig. 5. Waveform of the body motion accelerometer data, pertaining to arm swings of a subject during walk.

TABLE I
THE RECONSTRUCTED SNR FOR THE BIVARIATE DATA PERTAINING TO HUMAN WALK

Algorithm	Input SNR	Reconstructed SNR (dB)
MWSD	20dB	22.8
MWD	20dB	21.8
MFSD	20dB	21.2
MWSD	15dB	17.7
MWD	15dB	17.8
MFSD	15dB	18.3
MWSD	10dB	14.7
MWD	10dB	13.8
MFSD	10dB	15.5
MWSD	5dB	12.6
MWD	5dB	9.7
MFSD	5dB	12.2
MWSD	0dB	8.2
MWD	0dB	5.7
MFSD	0dB	8.1
MWSD	-5dB	3.16
MWD	-5dB	1.8
MFSD	-5dB	3.5

C. Human Motion Denoising

The data was obtained from the arm swings of a test subject using two 3D accelerometers attached to the wrists. A bivariate signal was then constructed (shown in Fig. 5) by using the y-axis accelerometer data (the y-axis of the accelerometer was perpendicular to ground, when the subject was at rest) collected from the left and right wrists of the test subject.

Fig. 5 shows that both the instantaneous frequency and amplitude of the bivariate accelerometer data are time-varying, also additive white Gaussian noise of varying powers was added to further complicate the recording. Table I shows that both of the proposed multivariate denoising algorithms (MWSD and MFSD) outperformed the MWD algorithm for input SNRs below 10 dB, while as expected at higher input SNRs the performances of all techniques were similar.

D. Float Drift Denoising

We next considered data collected from a freely drifting oceanographic float, that is used by oceanographers to study ocean current drifts.[8] The position (latitude and the longitude) of the float was recorded, and the resulting drift velocities for both the latitude and longitude were then used to construct a

[8]The float drift data is obtained from the Jlab toolbox, and is available at http://www.jmlilly.net. Data used for this simulation is available on request.

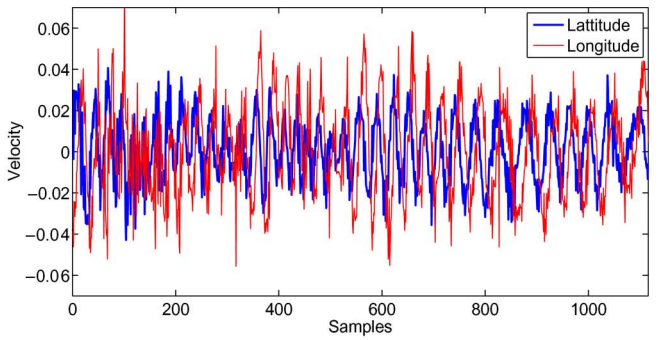

(a) Float Data

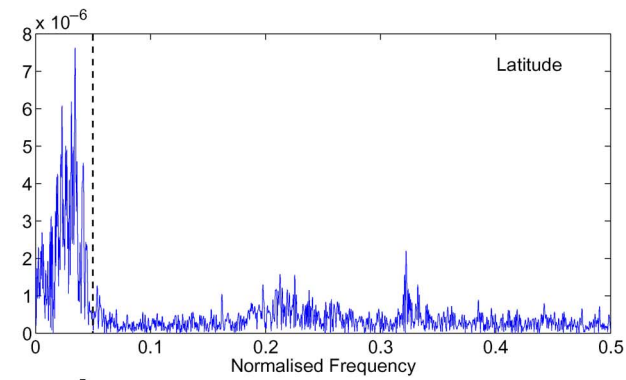

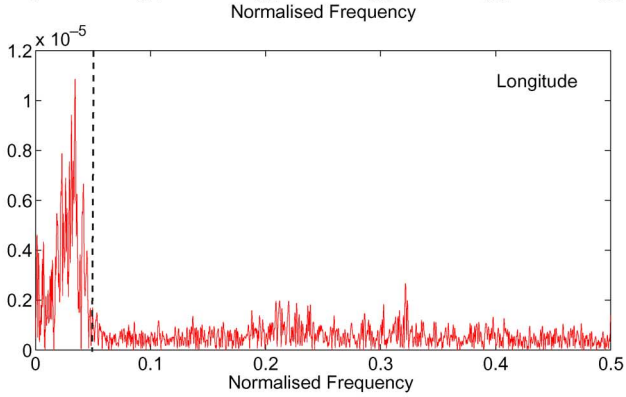

(b) Amplitude Spectra

Fig. 6. Oceanographic float drift recordings. (a) Time domain representation of the bivariate float drift data. (b) The amplitude spectra of the latitude (upper panel) and longitude (lower panel). (a) Float data; (b) amplitude spectra.

bivariate signal. Fig. 6(a) shows the time domain waveforms of the drift velocities for both the latitude and longitude; the bivariate signal contains a time-varying oscillation that is common to both channels with an approximately constant phase difference. Fig. 6(b) illustrates the respective amplitude spectra, showing that the oscillatory signals of interest reside within the frequency range [0,0.05], while the frequency content above the normalized frequency of 0.05 is due to white noise.

The resulting time domain representations of the denoised bivariate float data using both the proposed MWSD and the MWD algorithms are shown in Fig. 7(a); both algorithms correctly identified monocomponent bivariate oscillations; observe that the denoised float data estimated using the MWSD algorithm has smoother features over the MWD, while Fig. 7(b) presents the resulting amplitude spectra of the denoised signals. It can be seen that both methods preserved the frequency content below the normalized frequency of 0.05 and suppress the frequency content above the normalized frequency 0.05. Fig. 7(b) shows that the proposed MWSD algorithm outperformed the MWD for high frequency component suppression.

E. Denoising in Motor Imagery BCI

The final simulation considers the electroencephalography (EEG) data collected from a test subject performing motor imagery tasks. The objective of motor imagery (MI) experiments is to generate a response in the brain electrical activity when the subject imagines movement of a limb, manifested by a 10 Hz *mu* rhythm in EEG. A bivariate signal was constructed using two EEG electrodes FC3 and T7 (located on the left hemisphere of the skull), and the MI task involved the imagining left hand movement[9] [31]. The frequencies of interest for motor imagery tasks fluctuates in the range 8–12 Hz [32], and the physiological noise corrupting EEG signals tends to contain strong low frequency components, so that at the power spectra of EEG signals are proportional to the inverse of frequency $\left(\propto \frac{1}{f^{\alpha}}\right)$. To this end, the Hurst exponent value of $H = 0.995$ was used to model the noise characteristics of the motor imagery data.

Fig. 8(a) shows the time-frequency representations of the original EEG channels FC3 and T7; observe the presence of the *mu* rhythm along with strong background low frequency EEG components (at 0–4 Hz). Fig. 8(b) shows the denoised EEG using the MWSD algorithm; the *mu* rhythm was recovered while the low frequency background EEG components were removed.

VII. Conclusion

We have introduced a class of multivariate denoising algorithms based on synchrosqueezing in conjunction with the short time Fourier transform and the wavelet transform. By partitioning the time-frequency domain, a set of matched monocomponent signals has been obtained, while a multivariate extension of the thresholding method and a multivariate denoising algorithm have been proposed so as to exploit the inter-channel dependencies that exist between multiple data channels. Simulations on both synthetic and real world data have demonstrated the effectiveness of the proposed multivariate denoising methods. Finally, the proposed multivariate partitioning and denoising algorithms have also been applied to conventional time-frequency methods such as wavelet and short time Fourier transforms, and are advantageous for applications that require lower computational complexity over accurate signal recovery.

Appendix A

The implementation of the synchrosqueezing transform based on the STFT [21] is as follows.

A. STFT Implementation

The discrete implementation of the STFT (detailed in [27]), generally requires the specification of three parameters: 1) the type of window employed, 2) the window length used, and 3) the overlap between windows. For the first case, it has been shown that the Gaussian window, given by

$$w(n) = e^{-n_i^2/\alpha^2}, \tag{33}$$

[9]The data used in this simulation was obtained from the BCI Competition IV Dataset I, and is available from http://www.bbci.de/competition/iv/. Data used for this simulation is available on request.

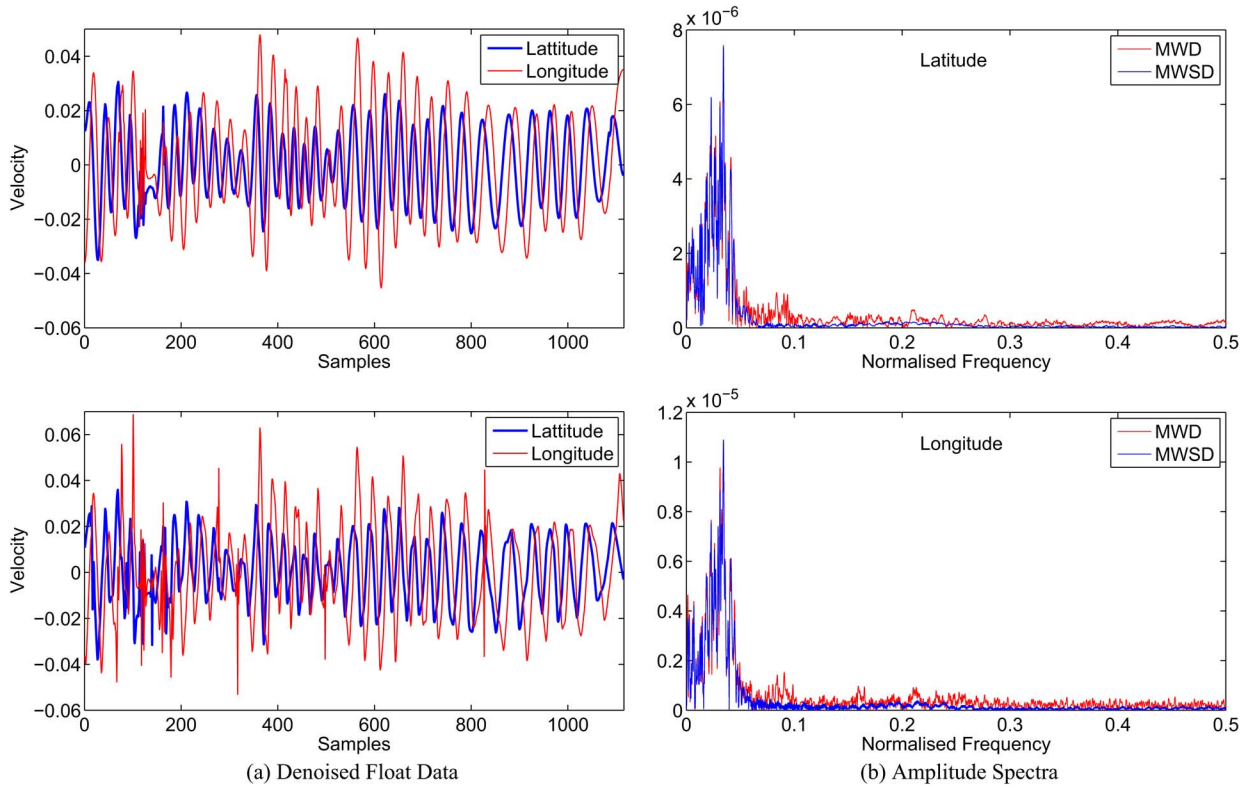

(a) Denoised Float Data (b) Amplitude Spectra

Fig. 7. Ocean float denoising. (a) The denoised bivariate float using the proposed MWSD method (upper panel) and the MWD algorithm (lower panel). (b) The amplitude spectra for both the MWSD and multivariate wavelet denoising algorithms for denoised signal corresponding to the latitude (upper panel) and the longitude (lower panel). (a) Denoised float data; (b) amplitude spectra.

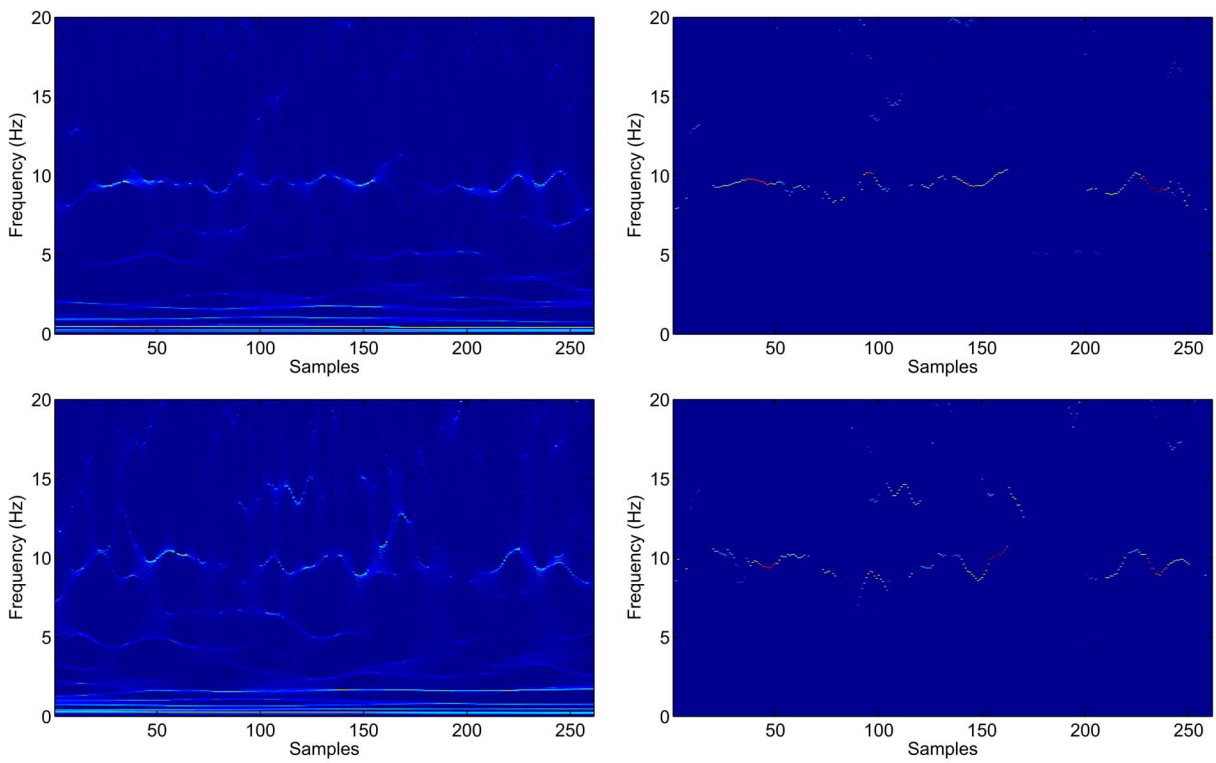

(a) Original FC3 and T7 electrodes (b) Denoised FC3 and T7 Electrodes

Fig. 8. Motor imagery denoising aiming to recover a drifting 10 Hz mu-rhythm from noisy EEG. (a) The time-frequency representations of EEG data pertaining to the left hand motor imagery, from the FC3 electrode (upper panel) and T7 electrode (lower panel). (b) The time-frequency representations of the denoised EEG signals using the MWSD algorithm, for the FC3 electrode (upper panel) and T7 electrode (lower panel). (a) Original FC3 and T7 electrodes; (b) denoised FC3 and T7 electrodes.

provides the best trade-off between both time and frequency localization, while for the third case, a sliding window is employed to allow for the reconstruction of the original signal, as well as providing information at each point in time. The

window length is effectively a parameter that controls the desired time and frequency resolution. A discrete implementation of the STFT is given in Algorithm 4.

Algorithm 4: Discrete implementation of the STFT

1) Given a discrete signal $x(n_t)$, where $n_t = 1, \ldots, N_t$, and a discrete Gaussian window function given by $w(p)$, where $p = 0, \ldots, P-1$, and the maximum of the window function is at $\lfloor \frac{P}{2} \rfloor$.
2) Zero pad each side of the signal $x(n_t)$ with $\lfloor \frac{P}{2} \rfloor$ zeros, yielding the following signal $x_z(n_t)$.
3) Next apply the discrete Fourier transform

$$S_i(n_t, k) = \mathcal{F}_d \left\{ \hat{x}_z(n_t) \odot \hat{w} \right\}, \quad \text{for} \quad n_t = 1, \ldots, N_t \tag{34}$$

where $\hat{x}_z(n_t) = [x_z(n_t), \ldots, x_z(n_t + P - 1)]^T$, $\hat{w} = [w(0), \ldots, w(P-1)]^T$, and $\odot$ corresponds to the elementwise product.

B. Instantaneous Frequency Estimation

Once the STFT coefficients $S_i(n_t, k)$ have been determined, the instantaneous frequency for each frequency index k needs to be calculated. An elegant solution (as outlined in [26] for the wavelet based SST) utilizes the derivative properties of the Fourier transform, that is, given the STFT coefficients, $S_i(n_t, k)$, apply the Fourier transform along the time dimension, yielding

$$B(n_t, \hat{k}) = \mathcal{F}_d \left\{ S_i(n_t, k) \right\}, \quad \text{for} \quad k = 0, \ldots, P-1 \tag{35}$$

By taking the inverse Fourier transform, $\mathcal{F}_d^{-1}\{\cdot\}$ of the following expression, we then obtain

$$\hat{\omega}(n_t, k) = \mathcal{F}_d^{-1} \left\{ \frac{i2\pi\hat{k}}{P} B(n_t, \hat{k}) \right\}, \quad \text{for} \quad \hat{k} = 0, \ldots, P-1 \tag{36}$$

yields the instantaneous frequency for each frequency index k.

C. STFT Synchrosqueezing

Finally, the discrete implementation of the synchrosqueezing for the STFT is given as follows. The inverse of the STFT coefficient, in a discrete implementation, is given by

$$x(n_t) = \frac{1}{Pw\left(\lfloor \frac{P}{2} \rfloor\right)} \sum_{k=0}^{P-1} S_i(n_t, k) \mathrm{e}^{i\pi k}. \tag{37}$$

This implies that the final reconstruction formula for the discrete implementation of the Fourier based synchrosqueezing transform is given by

$$T_d(n_t, k) = \frac{1}{Pw\left(\lfloor \frac{P}{2} \rfloor\right)} \sum_{k:\ |\hat{\omega}(n_t,k) - \omega_l| \leq \Delta\omega/2} S_i(n_t, k) \mathrm{e}^{i\pi k}, \tag{38}$$

for $k = 0, \ldots, P-1$.

Appendix B

Consider a bivariate frequency modulated signal given by

$$\mathbf{x}_+(t) = \begin{bmatrix} e^{i\phi(t)} \\ e^{i(\phi(t) + t\Delta)} \end{bmatrix}, \quad 0 \leq t \leq T, \tag{39}$$

where the instantaneous phase is given by, $\phi(t) = \sum_{h=1}^{H} c_h t^h$, where $c_h \in \mathbb{R}$. The objective is to determine the conditions under which the multivariate bandwidth, $\mathbf{B}_\mathbf{x}$, of the bivariate signal $\mathbf{x}_+(t)$, is greater than the sum of the individual channel-wise bandwidths $B_s = B_1 + B_2$, where B_1 and B_2 correspond to the bandwidth of each channel. Using (15)–(17) from Section III, the bandwidth for each separate channel is given by

$$B_1^2 = B_2^2 = \frac{1}{T} \int_0^T \left(\sum_{h=1}^{H} h c_h t^{h-1} - c_h T^{h-1} \right)^2 dt. \tag{40}$$

Accordingly the multivariate bandwidth of $\mathbf{x}_+(t)$ is given by

$$\mathbf{B}_\mathbf{x}^2 = \frac{1}{T} \int_0^T \frac{\Delta^2}{4} + \left(\sum_{h=1}^{H} h c_h t^{h-1} - c_h T^{h-1} \right)^2 dt. \tag{41}$$

In order to determine Δ so as to satisfy the following condition, $\mathbf{B}_\mathbf{x} > B_s$, that is, $\mathbf{B}_\mathbf{x}^2 > 4B_1^2$, which implies the following

$$\frac{1}{T} \int_0^T \frac{\Delta^2}{4} + \left(\sum_{h=1}^{H} h c_h t^{h-1} - c_h T^{h-1} \right)^2 dt > \frac{4}{T} \int_0^T \left(\sum_{h=1}^{H} h c_h t^{h-1} - c_h T^{h-1} \right)^2 dt. \tag{42}$$

In order to obtain a condition on Δ that satisfies (42), it is sufficient for Δ to satisfy the following

$$\frac{\Delta^2}{4} + \left(\sum_{h=1}^{H} h c_h t^{h-1} - c_h T^{h-1} \right)^2 > 4 \left(\sum_{h=1}^{H} h c_h t^{h-1} - c_h T^{h-1} \right)^2. \tag{43}$$

Rearranging (43) results in the following

$$\Delta > \sqrt{12} \left(\sum_{h=1}^{H} h c_h t^{h-1} - c_h T^{h-1} \right). \tag{44}$$

Given that instantaneous frequency $\phi'(t) = \sum_{h=1}^{H} h c_h t^{h-1}$, has some maximum value ω_{max} such that $\phi'(t) \leq \omega_{max}$, (44) can be expressed as follows

$$\Delta > \sqrt{12}(\omega_{max} - \overline{\omega}), \tag{45}$$

where $\overline{\omega} = \sum_{h=1}^{H} c_h T^{h-1}$. Implying that provided there exists sufficient frequency separation between bivariate frequency modulated oscillations, then the multivariate bandwidth using the method outlined in [28] enables the identification of modulated multivariate oscillations.

Appendix C

We shall now derive the variance of the partitioned coefficients $F_{n,v}(b)$ using synchrosqueezing techniques (where n corresponds to the channel index, while v is the oscillatory scale), starting from the wavelet based synchrosqueezing transform. The variance for each scale and channel is given by $\sigma_{n,v}^2 =$

$\mathrm{E}\{F_{n,v}(b)F^*_{n,v}(b)\}$. An approximation in order to simplify the derivation is given by

$$F_{n,v}(b) \approx R_\psi^{-1} \sum_{a\in A_v} a^{-\frac{3}{2}} W_d(a,b), \tag{46}$$

where $F_{n,v}(b)$ is the inverse of the wavelet transform within each frequency scale, and $A_v = \frac{\omega_\psi}{\omega_v}$, are the wavelet scale factors with center frequencies within the frequency partitions $\{\omega_v\}_{v=1,\ldots,V}$. Then, using (46) the variance within each frequency scale is given by

$$\sigma^2_{n,v} \approx R_\psi^{-2} \sum_{a\in A_v} a^{-3} \mathrm{E}\left\{W_d(a,b)W^*_d(a,b)\right\}. \tag{47}$$

Therefore, in order to calculate the variance, $\sigma^2_{n,v}$, for each scale and channel an expression needs to be determined for $\mathrm{E}\{W_d(a,b)W^*_d(a,b)\}$ (where $W_d(a,b)$ is the discrete time continuous wavelet transform). The first step is to carry out a change of variable of the continuous wavelet transform (shown in (19)),

$$W(a,b) = \int a^{-1/2}\psi^*\left(\frac{t}{a}\right) x(t+b)\, dt. \tag{48}$$

In discrete time, (48) is given by

$$W_d(a,b) = \sum_{m=0}^{L-1} a^{-1/2}\psi^*\left(\frac{m}{a}\right) x(m+b)\Delta t, \tag{49}$$

where L denotes the length of the signal, which yields

$$\begin{aligned}&\mathrm{E}\left\{W_d(a,b)W^*_d(a,b)\right\}\\ &\quad= \sum_{m_1=0}^{L-1}\sum_{m_2=0}^{L-1} a^{-1}\mathrm{E}\left\{x(m_1+b)x^*(m_2+b)\right\}\\ &\qquad\times \psi^*\left(\frac{m_1}{a}\right)\psi\left(\frac{m_2}{a}\right).\end{aligned} \tag{50}$$

Given a fractional Gaussian noise (fGn) signal, $x_H(k)$, with the following autocorrelation

$$\begin{aligned}&\mathrm{E}\left\{x_H(m)x_H(m+k)\right\}\\ &\qquad= \frac{\sigma_f^2}{2}\left(|k-1|^{2H} - 2|k|^{2H} + |k+1|^{2H}\right),\end{aligned} \tag{51}$$

where H is the Hurst exponent and σ_f corresponds to the standard deviation of the time series $x_H(m)$. A substitution between (51) and (50) gives

$$\begin{aligned}&\mathrm{E}\left\{W_d(a,b)W^*_d(a,b)\right\}\\ &= a^{-1}\frac{\sigma_f^2}{2}\sum_{m_1=0}^{L-1}\sum_{m_2=0}^{L-1}\left(|m_2-m_1-1|^{2H} - 2|m_2-m_1|^{2H}\right.\\ &\qquad\left.+|m_2-m_1+1|^{2H}\right)\psi^*\left(\frac{m_1}{a}\right)\psi\left(\frac{m_2}{a}\right)\end{aligned} \tag{52}$$

For white Gaussian noise with a Hurst exponent $H = 0.5$, expression (50) can be simplified into

$$\begin{aligned}&\mathrm{E}\left\{W_d(a,b)W^*_d(a,b)\right\}\\ &\quad= a^{-1}\sigma_w^2\sum_{m_1=0}^{L-1}\sum_{m_2=0}^{L-1}\delta(m_1-m_2)\psi^*\left(\frac{m_1}{a}\right)\psi\left(\frac{m_2}{a}\right)\\ &\quad= a^{-1}\sigma_w^2\sum_{m=0}^{L-1}\psi^*\left(\frac{m}{a}\right)\psi\left(\frac{m}{a}\right),\end{aligned} \tag{53}$$

where σ_w corresponds to the standard deviation of white noise. The final expressions for $\mathrm{E}\{W_d(a,b)W^*_d(a,b)\}$, determined for both fractional and white Gaussian noise are then substituted into (47), resulting in the variance for each oscillatory scale, $\sigma^2_{n,v}$, is given by

$$\begin{aligned}&\sigma^2_{n,v} \approx\\ &\quad= \frac{\sigma_f^2}{2R_\psi^2}\sum_{a\in A_v} a^{-4}\sum_{m_1=0}^{L-1}\sum_{m_2=0}^{L-1}\left(|m_2-m_1-1|^{2H}\right.\\ &\qquad\left.- 2|m_2-m_1|^{2H} + |m_2-m_1+1|^{2H}\right)\\ &\qquad\times\psi^*\left(\frac{m_1}{a}\right)\psi\left(\frac{m_2}{a}\right),\end{aligned} \tag{54}$$

The same reasoning applied to the STFT based synchrosqueezing transform yields the following estimates of the noise variance within each scale, where we first determine an expression assuming white noise

$$\sigma^2_{n,v} \approx \left(\frac{\sigma_w}{Pw\left(\left\lfloor\frac{P}{2}\right\rfloor\right)}\right)^2 \sum_{k\in A_s}\sum_{m=0}^{P-1} w(m)^2, \tag{55}$$

where $w(m)$ is the window of length P used in the STFT and A_s corresponds to the frequency partitions, $\{\omega_v\}_{v=1,\ldots,V}$, adapted for the STFT. For the fGn scenario, we then arrive at

$$\begin{aligned}\sigma^2_{n,v} \approx \left(\frac{\sigma_f}{Pw\left(\left\lfloor\frac{P}{2}\right\rfloor\right)}\right)^2 &\sum_{k\in A_s}\sum_{m_1=0}^{P-1}\sum_{m_2=0}^{P-1}\left(|m_2-m_1-1|^{2H}\right.\\ &\left.-2|m_2-m_1|^{2H} + |m_2-m_1+1|^{2H}\right)w(m_1)w(m_2).\end{aligned} \tag{56}$$

ACKNOWLEDGMENT

We wish to thank the anonymous reviewers for their valuable comments and suggestions.

REFERENCES

[1] B. Widrow, J. R. Glover, J. M. McCool, J. Kaunitz, C. S. Williams, R. Hearn, J. R. Zeidler, J. E. Dong, and R. C. Goodlin, "Adaptive noise cancelling: Principles and applications," *Proc. IEEE*, vol. 63, no. 12, pp. 1692–1716, 1975.

[2] D. L. Donoho and I. M. Johnstone, "Ideal spatial adaptation by wavelet shrinkage," *Biometrika*, vol. 81, pp. 425–455, 1994.

[3] Y. Kopsinis and S. McLaughlin, "Development of EMD-based denoising methods inspired by wavelet thresholding," *IEEE Trans. Signal Process.*, vol. 57, no. 4, pp. 1351–1362, 2009.

[4] A. To, J. Moore, and S. Glaser, "Wavelet denoising techniques with applications to experimental geophysical data," *Signal Process.*, vol. 89, no. 2, pp. 144–160, 2009.

[5] P. Ching, H. So, and S. Q. Wu, "On wavelet denoising and its applications to time delay estimation," *IEEE Trans. Signal Process.*, vol. 47, no. 10, pp. 2879–2882, 1999.

[6] D. Donoho, "De-noising by soft-thresholding," *IEEE Trans. Inf. Theory*, vol. 41, no. 3, pp. 613–627, 1995.

[7] M. Aminghafari, N. Cheze, and J.-M. Poggi, "Multivariate denoising using wavelets and principal component analysis," *Computat. Statist. Data Anal.*, vol. 50, no. 9, pp. 2381–2398, 2006.

[8] N. Huang, Z. Shen, S. Long, M. Wu, H. Shih, Q. Zheng, N. Yen, C. Tung, and H. Liu, "The empirical mode decomposition and the Hilbert spectrum for nonlinear and non-stationary time series analysis," *Proc. Royal Soc. A*, vol. 454, pp. 903–995, 1998.

[9] Q. Pan, L. Zhang, G. Dai, and H. Zhang, "Two denoising methods by wavelet transform," *IEEE Trans. Signal Process.*, vol. 47, no. 12, pp. 3401–3406, 1999.

[10] A. Boudraa and J. Cexus, "Denoising via empirical mode decomposition," in *Proc. ISCCSP*, 2006.
[11] N. Rehman and D. P. Mandic, "Multivariate empirical mode decomposition," *Proc. Royal Soc. A*, vol. 466, no. 2117, pp. 1291–1302, 2010.
[12] N. Rehman and D. P. Mandic, "Filter bank property of multivariate empirical mode decomposition," *IEEE Trans. Signal Process.*, vol. 59, pp. 2421–2426, 2011.
[13] F. Auger and P. Flandrin, "Improving the readability of time-frequency and time-scale representations by the reassignment method," *IEEE Trans. Signal Process.*, vol. 43, no. 5, pp. 1068–1089, 1995.
[14] F. Auger, P. Flandrin, Y.-T. Lin, S. McLaughlin, S. Meignen, T. Oberlin, and H.-T. Wu, "Time-frequency reassignment and synchrosqueezing: An overview," *IEEE Signal Process. Mag.*, vol. 30, no. 6, pp. 32–41, 2013.
[15] K. Kodera, R. Gendrin, and C. Villedary, "Analysis of time-varying signals with small BT values," *IEEE Trans. Acoust., Speech Signal Process.*, vol. 26, no. 1, pp. 64–76, 1978.
[16] I. Djurovic and L. Stankovic, "Time-frequency representation based on the reassigned s-method," *Signal Process.*, vol. 77, no. 1, pp. 115–120, 1999.
[17] I. Daubechies and S. Maes, "A nonlinear squeezing of the continuous wavelet transform based on auditory nerve models," in *Proc. Wavelets in Med. Biol.*, 1996, pp. 527–546.
[18] I. Daubechies, J. Lu, and H.-T. Wu, "Synchrosqueezed wavelet transforms: An empirical mode decomposition-like tool," *Appl. Computat. Harmonic Anal.*, vol. 30, no. 2, pp. 243–261, 2011.
[19] H.-T. Wu, P. Flandrin, and I. Daubechies, "One or two frequencies? The synchrosqueezing answers," *Adv. Adapt. Data Anal.*, vol. 3, no. 1–2, pp. 29–39, 2011.
[20] R. Carmona, W.-L. Hwang, and B. Torrésani, *Practical Time-Frequency Analysis*. New York, NY, USA: Academic, 1998.
[21] T. Oberlin, S. Meignen, and V. Perrier, "The Fourier-based synchrosqueezing transform," in *Proc. IEEE Int. Conf. Acoust., Speech, Signal Process.*, 2014, pp. 315–319.
[22] S. Meignen, T. Oberlin, and S. McLaughlin, "A new algorithm for multicomponent signals analysis based on synchrosqueezing: With an application to signal sampling and denoising," *IEEE Trans. Signal Process.*, vol. 60, no. 11, pp. 5787–5798, 2012.
[23] D. Gabor, "Theory of communication," *Proc. IEEE*, vol. 93, pp. 429–457, 1946.
[24] J. M. Lilly and S. C. Olhede, "Analysis of modulated multivariate oscillations," *IEEE Trans. Signal Process.*, vol. 60, no. 2, pp. 600–612, 2012.
[25] J. M. Lilly and S. C. Olhede, "Bivariate instantaneous frequency and bandwidth," *IEEE Trans. Signal Process.*, vol. 58, no. 2, pp. 591–603, 2010.
[26] G. Thakur, E. Brevdo, N. S. Fuckar, and H.-T. Wu, "The synchrosqueezing algorithm for time-varying spectral analysis: Robustness properties and new paleoclimate applications," *Signal Process.*, vol. 93, no. 5, pp. 1079–1094, 2013.
[27] L. Stanković, M. Daković, and T. Thayaparan, *Time-Frequency Signal Analysis With Applications*. Dedham, MA, USA: Artech House, 2013.
[28] S. Olhede and A. Walden, "The Hilbert spectrum via wavelet projections," *Proc. Royal Soc. A*, vol. 460, pp. 955–975, 2004.
[29] A. Ahrabian, D. Looney, L. Stankovic, and D. Mandic, "Synchrosqueezing-based time-frequency analysis of multivariate data," *Signal Process.*, vol. 106, pp. 331–341, 2015.
[30] G. Rilling, P. Flandrin, P. Goncalves, and J. M. Lilly, "Bivariate empirical mode decomposition," *IEEE Signal Process. Lett.*, vol. 14, no. 12, pp. 936–939, 2007.
[31] D. Mandic, N. Rehman, Z. Wu, and N. Huang, "Empirical mode decomposition-based time-frequency analysis of multivariate signals: The power of adaptive data analysis," *IEEE Signal Process. Mag.*, vol. 30, no. 6, pp. 74–86, 2013.
[32] C. Park, D. Looney, N. Rehman, A. Ahrabian, and D. P. Mandic, "Classification of motor imagery BCI using multivariate empirical mode decomposition," *IEEE Trans. Neural Syst. Rehab. Eng.*, vol. 21, no. 1, pp. 10–22, 2013.

Alireza Ahrabian received the M.Eng. degree in electrical and electronic engineering from Imperial College London, London, UK, in 2010, and the Ph.D. degree in time-frequency estimation, in 2014.

Currently, he is a Research Assistant in signal processing at Imperial College London. His research interests include time-frequency analysis and statistical signal processing.

Danilo P. Mandic (M'99–SM'03–F'12) received the Ph.D. degree in nonlinear adaptive signal processing from Imperial College London, London, U.K., in 1999.

He is a Professor of Signal Processing with Imperial College London, London, UK, where he has been involved in nonlinear adaptive signal processing and nonlinear dynamics. He has been a Guest Professor with Katholieke Universiteit Leuven, Leuven, Belgium, the Tokyo University of Agriculture and Technology, Tokyo, Japan, and Westminster University, London, UK, and a Frontier Researcher with RIKEN, Wako, Japan. He has two research monographs titled *Recurrent Neural Networks for Prediction: Learning Algorithms, Architectures and Stability* (West Sussex, UK: Wiley, 2001) and *Complex Valued Nonlinear Adaptive Filters: Noncircularity, Widely Linear and Neural Models* (West Sussex, UK: Wiley, 2009), an edited book titled *Signal Processing Techniques for Knowledge Extraction and Information Fusion* (New York, NY, USA: Springer, 2008), and more than 200 publications on signal and image processing.

Prof. Mandic has been a member of the IEEE Technical Committee on Signal Processing Theory and Methods, and an Associate Editor of the IEEE SIGNAL PROCESSING MAGAZINE, the IEEE TRANSACTIONS ON CIRCUITS AND SYSTEMS II, the IEEE TRANSACTIONS ON SIGNAL PROCESSING, and the IEEE TRANSACTIONS ON NEURAL NETWORKS. He has produced award winning papers and products resulting from his collaboration with the industry.